Available online at www.sciencedirect.com
ScienceDirect
Materials Chemistry and Physics 102 (2007) 225–230
MATERIALS CHEMISTRY AND PHYSICS
www.elsevier.com/locate/matchemphys

Powder property and electrochemical characterization of Li_2MnO_3 material

Sang-Ho Park [a], Yuichi Sato [b], Jae-KooK Kim [c], Yun-Sung Lee [d,*]

[a] *Argonne National Laboratory, 9700 S. Cass Avenue, Argonne, IL 60439, USA*
[b] *Department of Applied Chemistry, Kanagawa University, 3-27-1 Rokkakubashi, Yokohama 221-8686, Japan*
[c] *Department of Material Science and Engineering, Chonnam National University, 300 Yongbong-dong, Gwangju 500-757, Republic of Korea*
[d] *Faculty of Applied Chemical Engineering, Chonnam National University, 300 Yongbong-dong, Gwangju 500-757, Republic of Korea*

Received 9 July 2006; accepted 19 December 2006

Abstract

Li_2MnO_3 materials were synthesized at various calcination temperatures by the conventional solid state reaction. The Li_2MnO_3 powders were characterized by means of XRD, SEM, and TEM analyses. The particle properties of the Li_2MnO_3 powders, such as their surface morphology and oxygen content, as well as their electrochemical behaviors varied according to the calcinations temperatures. The discharge capacities of the Li/Li_2MnO_3 cells decreased with increasing calcination temperatures. The resulting Li_2MnO_3 material was mainly composed of Li_2MnO_3, sub-$LiMnO_2$, and sub-$LiMn_2O_4$ phases. The unexpected reversible discharge capacity of Li/Li_2MnO_3 cell fabricated in this study originated from the phase transformation between layered $LiMnO_2$ and cubic $LiMn_2O_4$ phases in this material.

Keywords: Li_2MnO_3; Phase transformation; Electrochemical properties; Cathode materials

1. Introduction

Lithium containing transition metal oxides $LiMO_2$ (M = Co, Ni, Mn) and the spinel $LiMn_2O_4$, have been extensively studied as a cathode material for commercial lithium secondary batteries. Mn-based oxides are promising candidates for cathode materials because of their low cost, abundance and nontoxicity [1,2]. Lithium manganese oxide, herein referred to as Li–Mn–O systems, are present in three different stoichiometries, viz. $LiMn_2O_4$ (cubic, *Fd*3*m*), $LiMnO_2$ (orthorhombic, *Pmnm* or monoclinic, *Pm*2*m*), and Li_2MnO_3 (monoclinic, *C*2/*m*). In the case of manganese spinel materials, lithium ions are reversibly inserted into and extracted out of the host cubic spinel phase in two composition ranges, $0 \le x \le 1$ and $1 \le x \le 2$, which produce two voltage plateaus at 4 V and 3 V, respectively [3,4]. The reversible capacity of manganese spinel materials originates from Mn^{3+}/Mn^{4+} redox reactions (the average Mn oxidation is +3.5). The other $LiMnO_2$ layered material have an Li_xMnO_2 stoichiometry, whose average Mn oxidation state was 3+, and their electrochemical capacity originated from Mn^{3+} to Mn^{4+} redox reactions. On the other hand, the oxidation state of Mn in Li_2MnO_3 is fixed at 4+, so this material does not show a electrochemical reaction, because the Mn^{4+} ion easily cannot be oxidized to the Mn^{5+} state. Recently, acid treatments were introduced to obtain electrochemically active $Li_{2-x}MnO_3$ materials [5,6]. Tabuchi et al. and Numata et al. [7,8] reported that the $LiFeO_2$–Li_2MnO_3 and $LiCoO_2$–Li_2MnO_3 solid solutions could be prepared by using hydrothermal-postannealing method and solid state methods, respectively.

In this work, Li_2MnO_3 monoclinic compounds were readily synthesized by the simple solid state reaction method from $LiOH{\cdot}H_2O$ and Mn_3O_4 starting materials. In the lower calcination temperature range, we have obtained a large surface area with a small particle size, and oxygen rich content (Li_2MnO_{3+y}). Unlike in previous reports, this Li/Li_2MnO_3 cell showed a high electrochemical reversible capacity in this study. Electrochemical characterizations of the Li_2MnO_3 material are presented herein along with the *ex situ* XRD and transmission electron microscopy (TEM) analysis, which show the structural evolution during the synthesis and cycling process.

2. Experimental

Li_2MnO_3 was synthesized by conventional solid state method using $LiOH{\cdot}H_2O$ (Kishida Chemical, Japan) and Mn_3O_4 (Tosho, Japan) as the

* Corresponding author. Tel.: +82 62 530 1904; fax: +82 62 530 1909.
E-mail address: leeys@chonnam.ac.kr (Y.-S. Lee).

0254-0584/$ – see front matter © 2006 Elsevier B.V. All rights reserved.
doi:10.1016/j.matchemphys.2006.12.008

starting materials. The stoichiometric amount of each material was grounded and calcined for 12 h at various temperatures (600–900 °C) under argon flow in the box furnace. The contents of Li and Mn in the resulting material were analyzed by atomic absorption spectroscopy (AAS, AA-6200, Shimadzu, Japan) by dissolving the powder in dilute nitric acid. Oxygen content was measured quantitatively using an oxygen determination analyzer (RO-416DR, EF-40C, LECO Corporation, USA). The specific surface area was measured in a Gemini 2375 instrument using the Brunauer, Emmett, and Teller (BET) method.

Powder X-ray diffraction (XRD, Rint 1000, Rigaku, Japan) using Cu Kα radiation was employed to identify the crystalline phase of the synthesized material. To investigate the structural difference of the positive electrode before and after cycling, each tested cell was left in a glove box for 2 days to reach equilibrium after cycling. The electrodes were washed with DMC solution to remove $LiPF_6$ salt. The particle morphology of the Li_2MnO_3 material was observed using a scanning electron microscope (SEM, S-4000, Hitachi Co., Japan). Transmission electron microscope (TEM, JEM 2010, JEOL, Japan) equipped with energy-dispersive X-ray spectrometer (EDS) was employed to characterize the microstructure of powder.

The electrochemical characterizations were performed using CR2032 coin-type cell. The cathode was fabricated with 20 mg of accurately weighed active material and 12 mg of conductive binder (8 mg of teflonized acetylene black (TAB) and 4 mg of graphite). It was pressed on 200 mm^2 stainless steel mesh used as the current collector under a pressure of 300 kg cm^{-2} and dried at 130 °C for 5 h in an oven. The test cell was made of a cathode and a lithium metal anode (Cyprus Foote Mineral Co.) separated by a porous polypropylene film (Celgard 3401). The electrolyte used was a mixture of 1 M $LiPF_6$–ethylene carbonate (EC)/dimethyl carbonate (DMC) (1:2 by vol., Ube Chemicals, Japan). The charge and discharge testing was applied with current density was 0.4 mA cm^{-2} with a cut-off voltage of 2.0–4.5 V at room temperature.

3. Results and discussion

Fig. 1 shows the XRD patterns of Li_2MnO_3 materials obtained at various calcination temperatures. All of the materials were indexed as a Li_2MnO_3 monoclinic structure with a space group of *C*2/*m*, which structure is the same as that of *R*3*m* layered rock-salt structures. However, Li_2MnO_3 has a different cation distributions in the transition metal site, in the form of an Mn_2Li mixed cation layer, which can expressed at $Li_{[3a]}(Li_{1/3}Mn_{2/3})_{[2b]}O_{2[6c]}$. As the calcination temperature increased, the diffraction peaks were quite sharper due to the high crystallinity of the Li_2MnO_3 powder. Well developed peaks in all synthesized materials at $2\theta = 64.5°$ and 65.5° corresponds (1 3 5) and (0 6 0) directions clearly remained, which indicated the degree of development of the monoclinic structure of Li_2MnO_3. However, the XRD pattern of the as-prepared samples calcined at 600 °C appears to be highly disordered, judging from the broadened peaks, containing a high density of stacking disorders. It was impossible to clearly distinguish the phase based on the X-ray diffraction patterns alone. It is difficult to obtain a clean diffraction pattern from the prepared at low temperature, due to the high degree of structural disorder induced by the small particle size, which caused by the relatively low calcination temperature.

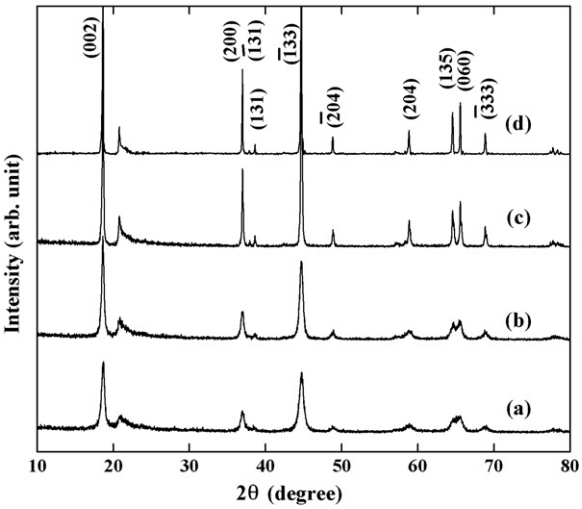

Fig. 1. X-ray diffraction patterns (XRD) of the Li_2MnO_3 powders prepared using different calcination temperatures. (a) 600 °C, (b) 700 °C, (c) 800 °C, and (d) 900 °C.

Table 1 shows the variation in the lattice constants of the resulting Li_2MnO_3 materials obtained at various temperatures. The lattice constants were calculated by the least square method from the XRD data in Fig. 1. As the calcination temperature increased, the lattice constant (a_h) slightly decreased from 4.939(6) for 600 °C to 4.934(0) Å for 900 °C. Because of the ionic radius of Mn^{3+} (0.65 Å) is larger than that of Mn^{4+} (0.53 Å), it can be inferred that the shortage (or complete absence) of Mn^{3+} ion in Li_2MnO_3 obtained at 900 °C resulted in the decrease of the lattice constant of the material obtained at high synthetic temperature. The larger lattice parameter a_h of Li_2MnO_3 obtained at lower calcination temperatures may be caused by presence of an oxygen rich phase, leading to the reduction of the average oxidation state of Mn in the final product. Although, in theory, the average oxidation state of Mn in the Li_2MnO_3 structure should be 4+, a small amount of Mn^{3+} may have formed at lower calcination temperature and participated in the electrochemical reaction. Moreover, the real oxygen content was determined to be Li_2MnO_{3+y} (rich oxygen phase) by the chemical analysis. Since these oxygen rich phases were caused by a reduction in the average Mn oxidation state in order to compensate for the total charge balance, the Mn^{3+} ions could participate in the charge/discharge reaction in the case of the Li_2MnO_3 obtained at lower synthetic temperatures.

Table 1
Calculated lattice constants and oxygen contents measured by chemical analysis

	a_h (Å)	b_h (Å)	c_h (Å)	β (θ)	Volume (Å^3)	Oxygen contents
600 °C	4.939(6)	8.540(2)	9.619(2)	99.98	400.17(1)	3.11
700 °C	4.938(7)	8.542(5)	9.634(9)	99.93	400.31(7)	3.06
800 °C	4.936(9)	8.541(1)	9.646(6)	99.87	400.60(1)	3.03
900 °C	4.934(0)	8.540(5)	9.638(4)	99.85	400.16(6)	3.01

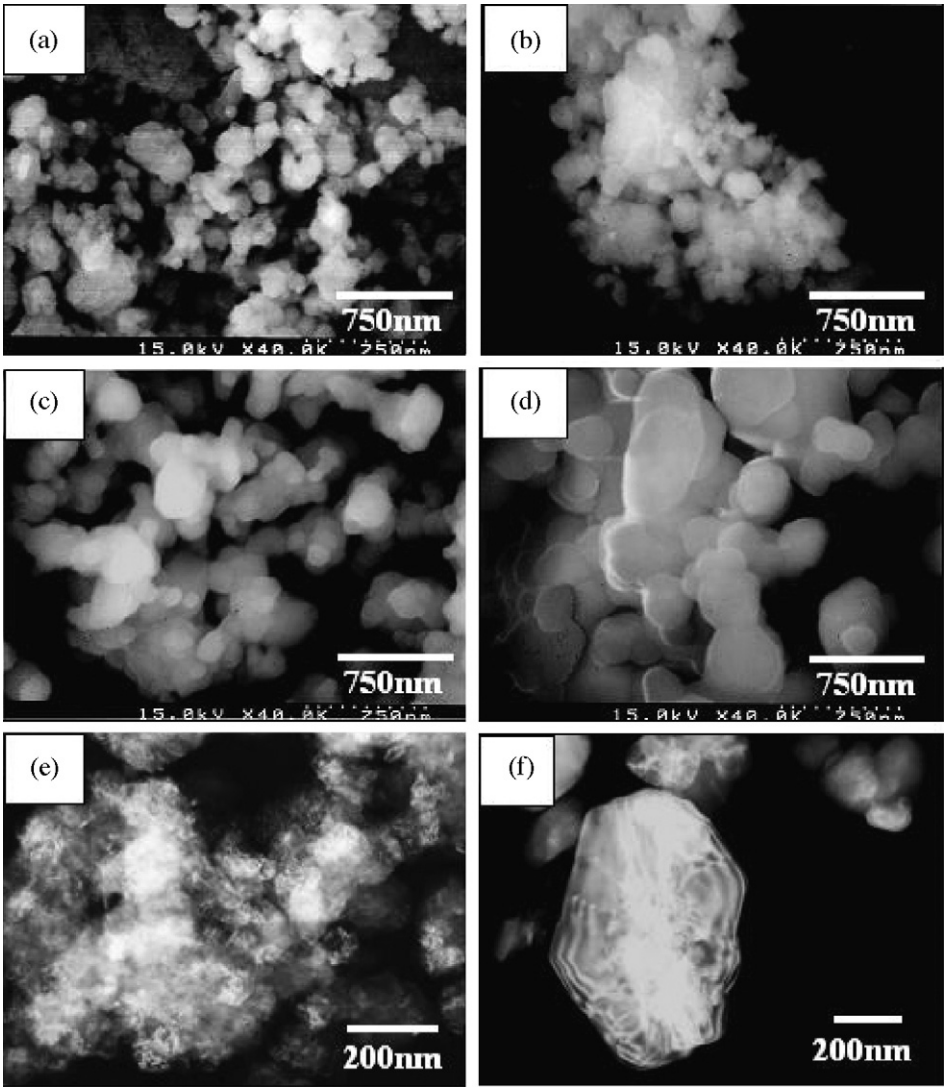

Fig. 2. SEM and TEM images of the as-prepared Li_2MnO_3 particles calcined at various temperatures. (a) 600 °C, (b) 700 °C, (c) 800 °C, (d) 900 °C (SEM), (e) 600 °C, and (f) 800 °C (TEM).

Fig. 2 shows the particle morphology of Li_2MnO_3 powders obtained at various calcination temperatures using scanning electron microscope (SEM) and transmission electron microscope (TEM). The observed particle sizes of the resulting powders increased with increasing calcination temperature. The powders prepared at lower temperature showed an agglomerated particle shape, and were primarily composed of 100–200 nm sized particles. However, the calcination at higher temperature resulted in the growth of crystallite which merged with each other to form agglomerations, as shown in Fig. 2(c) and (d). Furthermore, the difference in the primary particles and porosity between the low and high temperature synthesis are clearly confirmed by TEM results as shown in Fig. 2(e) and (f), respectively.

Fig. 3 shows the relationship between the synthesis temperature and specific surface area measured using BET analysis. The specific surface area is strongly affected by the surface morphological chemistry during the synthetic processing condition. As the calcination temperatures increased, the surface areas decreased in this study. When the calcination temperature

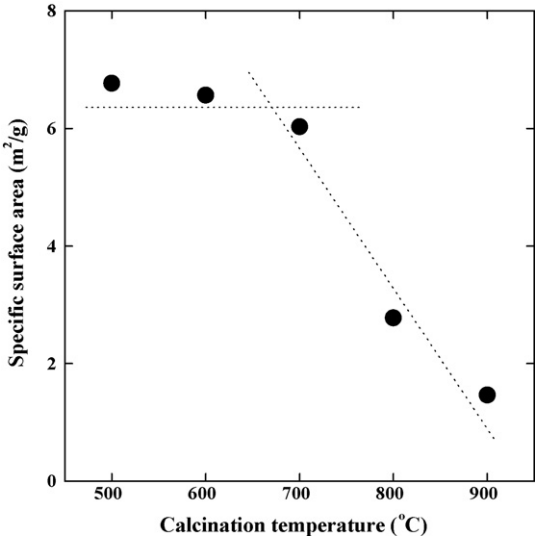

Fig. 3. Specific surface area of the Li_2MnO_3 powders obtained at various calcination temperatures.

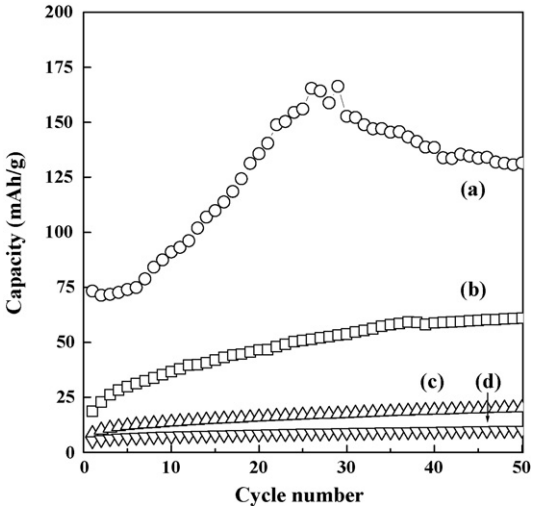

Fig. 4. A plot of the specific discharge vs. number of cycles for the Li/1 M $LiPF_6$-EC/DMC/Li_2MnO_3 cells obtained at various calcination temperatures. (a) 600 °C, (b) 700 °C, (c) 800 °C, and (d) 900 °C. The test condition was a current density of 0.4 mA cm^{-2} between 4.5 V and 2.0 V at room temperature.

was over 800 °C, the surface area was dramatically decreased until 3.0 $m^2\,g^{-1}$. Materials with larger surface area, low crystallinity, and small crystalline size have more electrochemical reaction spots during charge/discharge process. Consequently, the Li_2MnO_3 prepared at low calcination temperature could show higher discharge capacity than that of the samples prepared at a higher temperature. The relation between the surface area and discharge capacity was reported in previous studies of the effects of ball milling [9,10].

Fig. 4 shows the specific discharge capacity versus the number of cycles of the Li/Li_2MnO_3 cells cycled between 2.0 V and

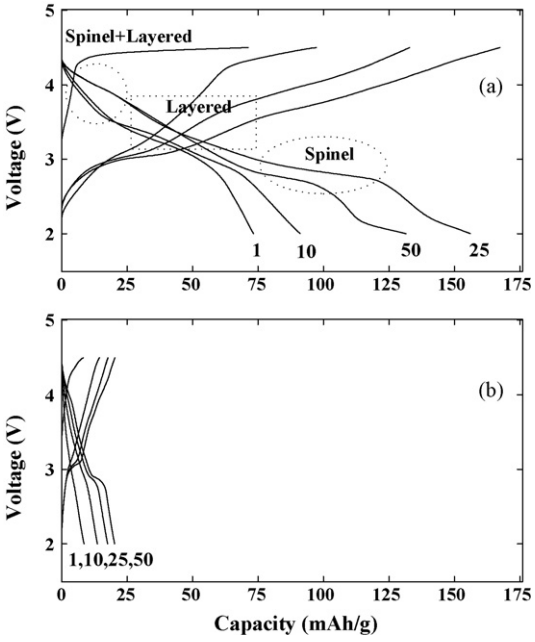

Fig. 5. The charge/discharge curves for the Li/1 M $LiPF_6$-EC/DMC/Li_2MnO_3 cells obtained at (a) 600 °C and (b) 800 °C. The test condition was a current density of 0.4 mA cm^{-2} between 4.5 V and 2.0 V at room temperature.

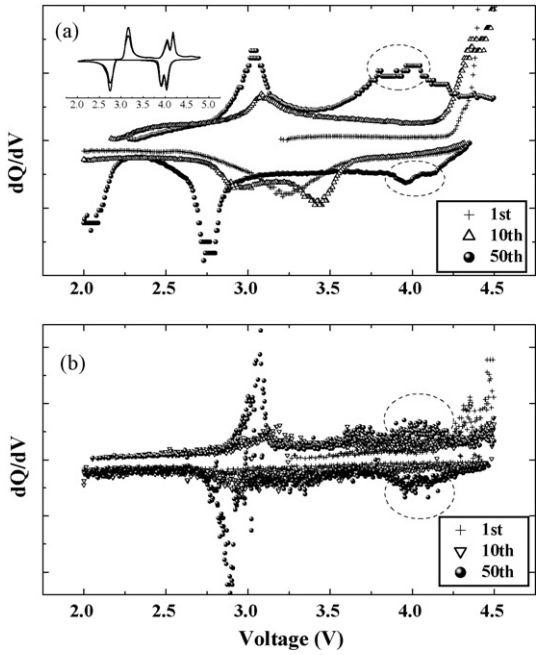

Fig. 6. Differential capacity vs. voltage profiles for the Li/Li_2MnO_3 cells obtained at (a) 600 °C and (b) 800 °C. The inset shows the differential capacity vs. voltage profile for the Li/$LiMn_2O_4$ cell.

4.5 V at a constant current density of 0.4 mA cm^{-2} at 25 °C. It is well-known that the stoichiometric Li_2MnO_3 material commonly shows no electrochemical reaction. Because its charge balance can be expressed as $Li_2{}^{1+}Mn^{4+}O_3{}^{2-}$, it is difficult for the lithium ions to insert/extract in the Mn layers between 2.0 V and 4.5 V windows. However, the Li/Li_2MnO_3 cell obtained at 600 °C shows an initial charge/discharge capacity (75 mAh g^{-1}) in the first cycle, and then, the capacity was drastically increased up to about 150 mAh g^{-1} at 25th cycle. On the other hand, the reversible discharge capacity of Li/Li_2MnO_3 cells obtained at over 700 °C decreased from 20 mAh g^{-1} to 10 mAh g^{-1} with increasing temperatures. It is possible that the discharge capacity of the Li/Li_2MnO_3 cells in this study is related to reduction

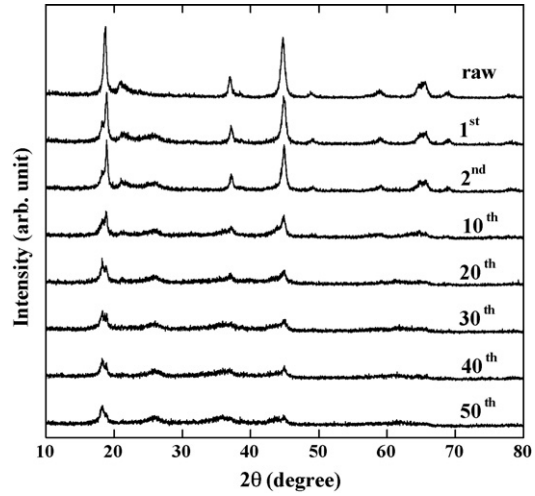

Fig. 7. XRD pattern of the as-prepared Li_2MnO_3 obtained at 600 °C and *ex situ* XRD patterns of Li_2MnO_3 electrodes in discharge state after various cycles.

and/or oxidation of Mn ions between 4+ and 3+ during electrochemical cycling.

Fig. 5(a) and (b) shows the charge/discharge curves of Li/Li_2MnO_3 electrodes obtained at 600 °C and 800 °C, respectively. The charge/discharge current density was 0.4 mA cm^{-2} between 2.0 V and 4.5 V. The shape of charge/discharge curves for the two cells might be shown that the layered and spinel composite electrodes. These two cells show almost the same shape of charge/discharge curves, although there was a big difference in capacities, with both spinel ($LiMn_2O_4$) and layered (orthorhombic or monoclinic-$LiMnO_2$) types, respectively. The initial discharge curves of two cells in the 4 V regions could be considered to show the existence and participation of spinel and layered type composite electrodes during cycling. Moreover diagonal shape of voltage curves between 4 V and 3 V are very similar with the typical Li/Li_xMnO_2 (O_3 type layered) or orthorhombic $LiMnO_2$ electrode cell [11,12]. As more lithium ions are inserted into the host structure, the voltage profile undergoes another distinguished voltage plateau around at 3 V. The 3 V plateau is one of the characteristics of the spinel phase, $Li_{1+x}Mn_2O_4$, wherein lithium ions are inserted into the octahedral sites. Notice that the 4 V and 3 V plateau in the charge/discharge curves becomes increasingly flatter with further cycling, which suggests that the structure has slowly

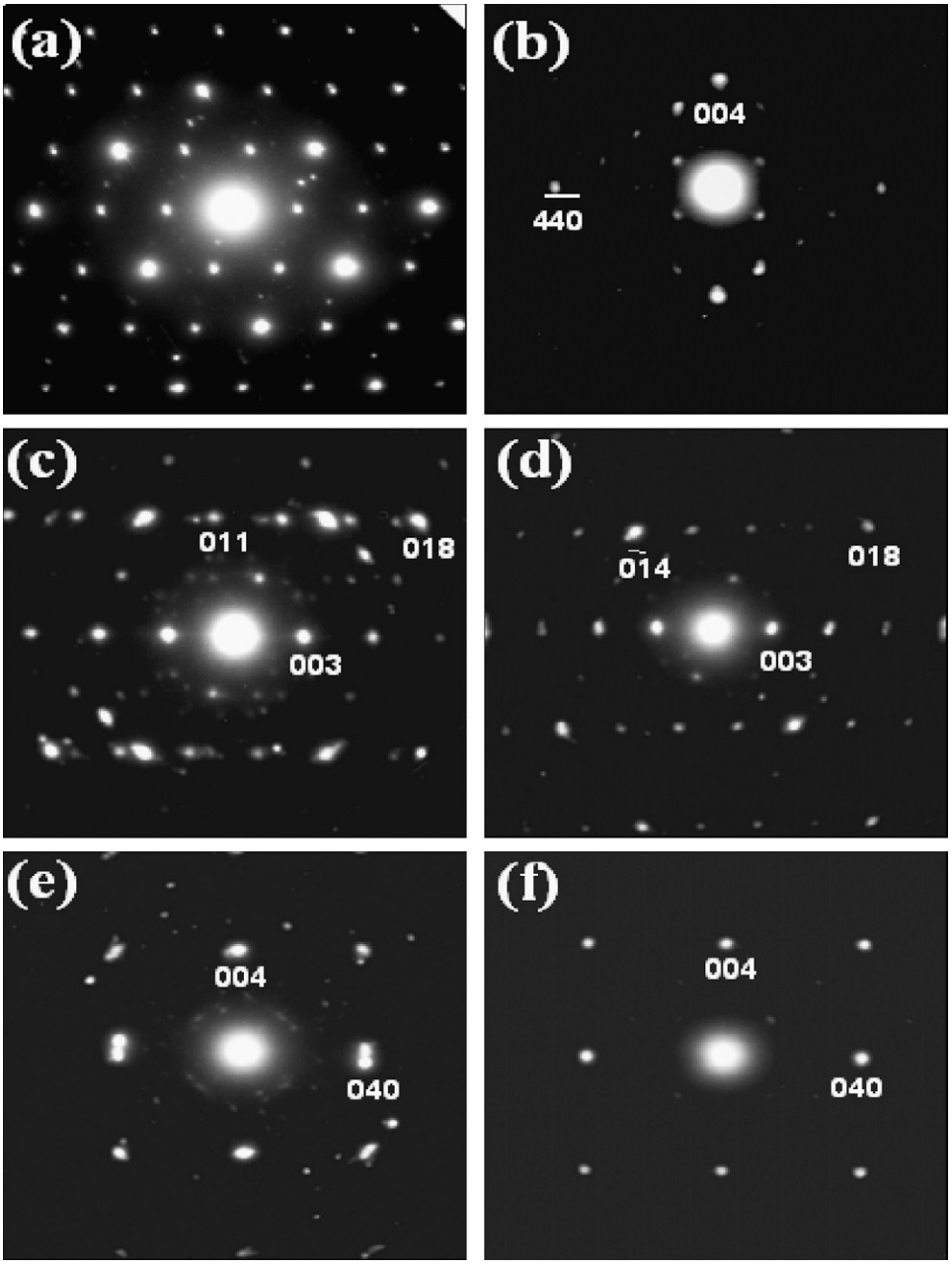

Fig. 8. SAD patterns (zone 100) of the Li_2MnO_3 electrode obtained at 600 °C. (a), (c), and (e) were recorded before the cycling of the electrode, and indicate the Li_2MnO_3, $LiMnO_2$, $LiMn_2O_4$ phases, respectively, (b), (d), and (f) were recorded after the cycling of the electrode, and indicate the Li_2MnO_3, $LiMnO_2$, $LiMn_2O_4$ phases, respectively.

transformed into the spinel structure. The observation is in agreement with the previous reports that the layered Li_xMnO_2 transformed to spinel phase during lithium insertion/extraction in the structure [13,14]. It is speculated that the electrochemical cycling behavior of the Li_2MnO_3 electrode can partly attributed to the formation of a composite structure, which can be assumed by $0.6Li_2MnO_3$–$0.4LiMn_2O_4$ electrode. This value can be calculated based on the first discharge electrochemical capacity for 600 °C sample.

Fig. 6 shows the differential capacity versus voltage profiles of Li/Li_2MnO_3 cells obtained at various synthetic temperatures in the potential range of 2.0–4.5 V. The Li/$LiMn_2O_4$ cell is also presented in the inset Fig. 6 for the comparison. The differential capacity of Li_2MnO_3 material obtained at 600 °C has only one redox peak in the first cycle, as shown in Fig. 6(a). The single redox peak gradually divides into two redox peaks situated at around 3 V and 3.5 V, respectively. Each of these two peaks is further split, shown to lower and higher voltage regions, at around 4 V peaks dividing after the 50th cycle, which well match on the normal spinel $LiMn_2O_4$ properties as like as two clear redox couples at 3.95 V and 4.1 V as shown inset figure. Accordingly, this result suggests that the insertion/extraction of lithium ions occurs in a multi-stage phase transition from layered to spinel structures.

In order to investigate the structural change of Li_2MnO_3 samples before and after cycling, *ex situ* XRD measurements were taken of seven Li_2MnO_3 electrodes in the discharged state after various numbers of cycles, as shown in Fig. 7. Each cell was left in a glove box for 2 days to reach equilibrium after being tested from 2.0 V to 4.5 V. The second separation from the Li_2MnO_3 host material occurred after the first cycle, followed by the appearance of another phase at lower angle. Moreover, the fraction of original phase considerably decreased when the electrode was cycled for more than 20 cycles, whereas the newly formed phase was increased, as can be seen in Fig. 8. Especially, the super lattice structure (1 1 1), (0 2 0) peaks at around $2\theta = 21^\circ$ and (1 3 5), (0 0 6) peaks at around $2\theta = 64^\circ$ were remarkably diminished after 30 cycles, which means that irreversible phase transformation occurred due to participating electrochemical reaction of electro active Li_2MnO_3. Unfortunately, it is impossible to define structural refinements clearly, due to the lower crystallininty. However, we could find that this new structure might consist of $Li_xMn_2O_4$ and $LiMnO_2$ (O_3 type or orthorhombic) structures.

The microstructures of the as-prepared materials and cycled electrodes were examined using transmission electron microscopy (HR-TEM), as shown in Fig. 8. In agreement with the *ex situ* XRD result and electrochemical analysis, the electron diffraction pattern of the as prepared particles indicated that the main phase is Li_2MnO_3. We also found small fractions of $LiMnO_2$ and $LiMn_2O_4$ phases in the as-prepared particles. However, after charge/discharge cycling, the sub-phases in the cycled electrodes contained a small fraction of $LiMnO_2$ and $LiMn_2O_4$ phases. We are unsure of the exact fraction of the tetragonal phase, which resulted from the transformation of spinel $LiMn_2O_4$ phase, due to the limited number of particles examined using TEM. However, we believe that the fraction should be negligible, since the XRD data did not show presence of appreciable amount of the layered $LiMnO_2$ and $LiMn_2O_4$ spinel phases. The diffraction patterns indicate that the defected Li_2MnO_3 structure may also be transform into the $LiMnO_2$ and $LiMn_2O_4$ symmetry. We suggested that the observed electrochemical capacity in the Li/Li_2MnO_3 cell might have been brought about by the presence of impurity phase, such as partially ordered $LiMnO_2$ and $LiMn_2O_4$ phases in the resulting material.

4. Conclusion

Li_2MnO_3 powders were prepared by the conventional solid state reaction method. We investigated the electrochemical properties and structural changes of the Li/Li_2MnO_3 cells during lithium insertion/extraction process. The Li_2MnO_3 obtained at various calcination temperatures exhibited different surface morphologies, oxygen contents, and electrochemical reversible capacities. The materials calcined at lower temperature have a large specific surface area, low crystallinity and smaller particles size than those prepared at higher temperatures. Using the XRD, differential capacity analysis, and HRTEM tools, it was found that the Li_2MnO_3 obtained at 600 °C was mainly composed of Li_2MnO_3, sub-$LiMnO_2$, and sub-$LiMn_2O_4$ phases in the structure. Moreover, Li_2MnO_3 materials were transformed between $LiMnO_2$ layered and $LiMn_2O_4$ cubic phases during lithium insertion/extraction process.

Acknowledgements

This work was supported by the Core Technology Development Program of the Ministry of Commerce, Industry and Energy (MOCIE).

References

[1] F. Capitaine, P. Cravereau, C. Delmas, Solid State Ionics 89 (1996) 197.
[2] A.R. Armatrong, P.G. Bruce, Nature 381 (1996) 499.
[3] T. Ohzuku, M. Kitagawa, T. Hirai, J. Electrochem. Soc. 137 (1990) 769.
[4] M.M. Thacheray, J. Electrochem. Soc. 142 (1995) 2558.
[5] Y. Shao-Horn, Y. Ein-Eli, A.D. Robertson, W.F. Averill, S.A. Hachney, W.F. Howard Jr., J. Electrochem. Soc. 145 (1998) 16.
[6] C.S. Johnson, S.D. Korte, J.T. Vaughey, M.M. Thacheray, T.E. Bofinger, Y.S. Hao-Horn, S.A. Hachney, J. Power Sources 81/82 (1999) 491.
[7] M. Tabuchi, A. Nakashima, H. Shigemura, K. Ado, H. Kobayashi, H.S. Akaebe, H. Kageyama, T. Nakamura, M. Kohzaki, A. Hirano, R. Kannoe, J. Electrochem. Soc. 149 (2005) A509.
[8] K. Numata, S. Yamanaka, Solid State Ionics 118 (1999) 117.
[9] Y.S. Lee, C.S. Yoon, Y.K. Sun, M. Yoshio, Electrochem. Solid State Lett. 5 (2002) A1.
[10] Y.-I. Jang, B. Huang, Y.-M. Chiang, D.R. Sadoway, Electrochem. Solid State Lett. 1 (1998) 13.
[11] T.E. Quine, M.F. Duncan, A.R. Armstrong, A.D. Robertson, P.G. Bruce, J. Mater. Chem. 10 (2000) 2828.
[12] G. Vitins, K. West, J. Electrochem. Soc. 144 (1997) 2587.
[13] Y. Shao-Horn, S.A. Hachney, A.R. Armstrong, P.G. Bruce, R. Gitzendanner, C.S. Johnson, M.M. Thackeray, J. Electrochem. Soc. 146 (1999) 2404.
[14] Y. Jang, F.C. Chou, B. Huang, D.R. Sadoway, Y.-M. Chiang, J. Phys. Chem. Solids 64 (2003) 2525.